Available online at www.sciencedirect.com

SciVerse ScienceDirect

Ceramics International 39 (2013) 8327–8333

CERAMICS INTERNATIONAL

www.elsevier.com/locate/ceramint

X-ray diffraction, Raman and photoluminescence studies of nanocrystalline cerium oxide thin films

G. Balakrishnan[a,*], C.M. Raghavan[b], C. Ghosh[c], R. Divakar[c], E. Mohandas[c], Jung Il Song[a,*], S.I. Bae[a], Tae Gyu Kim[d]

[a]Department of Mechanical Engineering, Changwon National University, Changwon 641773, South Korea
[b]Department of Physics, Ferroelectrics Thin film Laboratory, Changwon National University, Changwon 641773, South Korea
[c]Materials Synthesis and Structural Characterisation Section, Physical Metallurgy Group, Indira Gandhi Centre for Atomic Research, Kalpakkam 603102, India
[d]Department of Nanomechatronics Engineering, Pusan National University, Miryang-si 627706, South Korea

Received 31 January 2013; received in revised form 15 March 2013; accepted 15 March 2013
Available online 11 April 2013

Abstract

Cerium oxide (CeO_2) thin films were deposited on Si (100) and glass substrates at various oxygen partial pressures (2×10^{-5} mbar–3×10^{-1} mbar) and a substrate temperature of 673 K, by pulsed laser deposition (PLD). The structural, morphological and optical properties of the films were characterized by X-ray diffraction, Raman spectroscopy, high resolution transmission electron microscopy, atomic force microscopy, photoluminescence and UV–visible spectroscopy. XRD analysis revealed the polycrystalline and cubic structure of the CeO_2 films with preferred orientation for (200) as the increase of oxygen partial pressure. The Raman studies indicated the formation of Ce–O with the systematic variation of peak intensity and FWHM with oxygen partial pressures. The high resolution transmission electron microscopy investigation confirmed the polycrystalline and cubic nature of the CeO_2 films with (200) preferred orientation. The AFM studies showed the roughness (RMS) values of the films increased from 0.8 nm to 4.6 nm with increasing oxygen partial pressure from 2×10^{-5} mbar to 3×10^{-1} mbar. The photoluminescence (PL) investigation indicated the bandgap values in the range 3.05–3.10 eV with increasing oxygen partial pressures. The UV–visible spectroscopy analysis demonstrated that the refractive index of the films decreased from 2.41 to 1.72 with increasing oxygen partial pressures.

Keywords: X-ray diffraction; Thin films; Cerium oxide; Raman spectroscopy; Photoluminescence

1. Introduction

Cerium oxide (CeO_2) thin film is of great interest due to its excellent properties such as high refractive index, wide bandgap, high dielectric constant, high melting point, high transparency in the VIS–NIR regions with high thermal and chemical stability [1,2]. These properties enhance the use of CeO_2 films for various electronic applications, such as silicon-on-insulator structure, miniaturized stable capacitors and buffer layers for the high temperature superconductor films [3,4]. CeO_2 films are also used in single and multilayer coatings for optical devices, electro-chromic windows, sensors and high temperature oxidation resistant coatings [5–7]. It is widely used as UV blocking filters in medical glassware and aerospace windows due to strong absorption in ultraviolet region [8]. High quality CeO_2 films have interesting optical properties for application as counter electrodes in transparent opto-ionic devices. It is a promising material for fast oxygen sensors at high temperature, because of its chemical stability and high diffusion coefficient of oxygen vacancies. Doped and undoped CeO_2 are important luminescent materials and investigated for optical marker, biological labeling and phosphor applications [9,10]. CeO_2 thin films are prepared by several methods, such as spray pyrolysis [11], electron-beam evaporation [12], sputtering [13], electro deposition [14] and pulsed

*Corresponding authors.
E-mail addresses: bala_physics76@yahoo.co.uk, balaphysics76@gmail.com (G. Balakrishnan), jisong@changwon.ac.kr (J.I. Song).

0272-8842/$ - see front matter © 2013 Elsevier Ltd and Techna Group S.r.l. All rights reserved.
http://dx.doi.org/10.1016/j.ceramint.2013.03.103

laser deposition (PLD) [15,16]. Among these methods, PLD is a simple and unique technique to prepare high quality thin films of metals, semiconductors and insulators [16]. One of the main advantages of PLD is the generation of hyperthermal species with high kinetic energy of the order of 100 eV [17]. Deposition of hyperthermal species can enhance the adatom mobility and hence the film quality. In the PLD process, there are several operating parameters such as wavelength, fluence, repetition rate, energy per pulse, ambient gases, pressure of the ambient gases, target to substrate distance and substrate temperature. Among these parameters, oxygen partial pressure and substrate temperature have profound influence on the properties. Hence, the present work deals with the influence of oxygen partial pressure on microstructural and optical properties of CeO_2 thin films.

2. Experimental details

CeO_2 (99.99% purity) powder was compacted into a pellet of 25 mm diameter and 4 mm thickness using a uni-axial press. The pellet was sintered at 1673 K for 6 h and used as target for preparation of thin films. Deposition of CeO_2 films on clean Si (100) and glass substrates was carried out as a function of oxygen partial pressure (2.0×10^{-5}–3.0×10^{-1} mbar) at 673 K, using KrF (248 nm) excimer laser with the energy density of 3 J/cm^2. The other deposition parameters are given elsewhere [15]. The structural property of the films was studied by X-ray diffractometer (X'pert PW 3040 D-8, PANalytical) using Cu $K_{\alpha 1}$ radiation.

The crystalline sizes were determined from the XRD data using Scherrer formula:

$$D = \frac{K\lambda}{\beta Cos\theta}$$

where $\beta = \sqrt{(B^2 - b^2)}$ K is Scherrer constant (0.9), λ is the wavelength of the $CuK_{\alpha 1}$ radiation, D is the crystallite size, β is full width at half maximum (FWHM) after correcting for instrumental broadening, θ is the diffraction angle, B is the observed FWHM of the film and b is the instrumental broadening. The structural property was also examined by Raman spectrophotometer (NRS-3300) at room temperature and ambient air. The Nd-YAG laser of 7.7 mW power with a wavelength of 532 nm was used as the excitation source. A high resolution transmission electron microscope (HRTEM) study of the CeO_2 film was carried out by a JEOL 2000 EX II (T) transmission electron microscope operated at 200 kV. The surface morphology and RMS surface roughness of the films was analyzed by atomic force microscope (AFM) (XE-100 Park systems). Room temperature photoluminescence (PL) was recorded using T64000 Jovin–Yvon spectrometer with a CCD detector and 1800 g/mm grating. A He–Cd laser of wavelength 325 nm, was used as the excitation source. The optical properties was studied by UV–VIS–NIR (Model no.: 3101/PC, Shimadzu) spectrophotometer in the wavelength range 190–800 nm. The refractive indices of films were calculated from transmittance spectra using the following equation:

$$n = [N + (N^2 - n_0^2 n_1^2)^{1/2}]^{1/2}$$

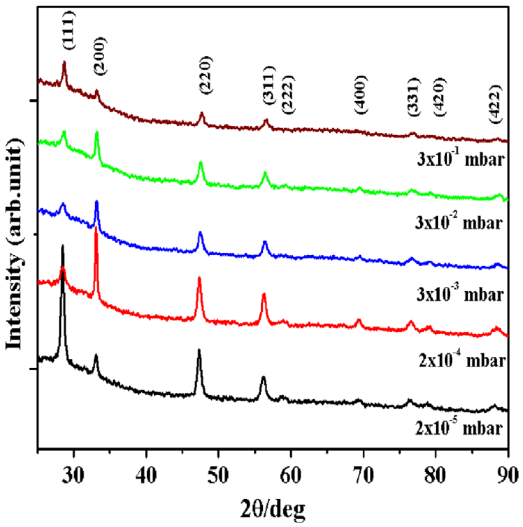

Fig. 1. XRD pattern of ceria films deposited on glass substrates at various oxygen partial pressures and 673 K.

Table 1
Oxygen partial pressure versus crystallite size, Raman FWHM and refractive index.

Sl. no.	Oxygen partial pressure (mbar)	Crystallite size (nm) (111)	Crystallite size (nm) (200)	FWHM from Raman (cm^{-1})	Refractive index at 550 nm
1	2.0×10^{-5}	25	24	12.54	2.41
2	2.0×10^{-4}	12	45	15.29	2.34
3	3.0×10^{-3}	7	28	10.10	1.91
4	3.0×10^{-2}	11	24	9.79	1.77
5	3.0×10^{-1}	32	19	–	1.72

where

$$N = \frac{n_0^2 + n_1^2}{2} + 2n_0 n_1 \frac{T_{max} - T_{min}}{T_{max} T_{min}}$$

where n is the refractive index of the film, n_o is the refractive index of air, n_1 is the refractive index of the substrate, T_{max}, T_{min} are the maximum and minimum transmittance respectively.

3. Results and discussion

3.1. Microstructural characterization

3.1.1. X-ray diffraction studies

Fig. 1 shows the XRD pattern of the CeO_2 films deposited on glass substrates at various oxygen partial pressures. The films showed (111), (200), (220), (311), (400), (331), (420) and (422) reflections correspond to the polycrystalline cubic structure of CeO_2 [18,19]. The films showed higher intensity for (111) reflection at base vacuum of 2.0×10^{-5} mbar. There was an increased intensity for (200) reflection at higher oxygen partial pressure (2×10^{-4}–3.0×10^{-2} mbar), whereas the intensity of (111) reflection decreased simultaneously, which indicates the preferred orientation of the films with increasing oxygen partial pressure [20,21]. The thickness of the films was measured and

found to decrease from 300 nm to 70 nm with increasing oxygen partial pressures. This is due to the increased scattering of ablated species with oxygen molecules in the deposition chamber. The peak intensity of all the reflections decreased at an oxygen partial pressure of 3×10^{-1} mbar, due to the reduced thickness. The crystallite size was calculated from Scherrer's equation after subtracting the instrumental broadening (Table 1). Kanakaraju et al. [21] investigated the properties of CeO_2 films prepared on fused silica substrates as a function of oxygen partial pressure and observed the texture of (200) in the temperature ≥400 °C. Amirhaghi et al. [22], grown the CeO_2 films on Si (100) substrates at different oxygen partial pressure and temperature using PLD and revealed that the films deposited at lower oxygen partial pressure, high substrate temperature and the laser fluence > 2 J cm^{-2} were good quality films. Wang et al. [20] studied the CeO_2 films deposited on Si (100) and found that the films orientation varied with increasing oxygen pressure.

3.1.2. Raman spectroscopy studies

The Raman spectroscopy was used to study the structure of the films deposited on Si (100). In general, CeO_2 has a fluorite structure and six optical phonon modes, which gives three zone center frequencies, 272, 465 and 595 cm^{-1} correspond to doubly degenerate transverse optical (TO) mode, triply degenerate and the non-degenerate longitudinal optical (LO) mode. CeO_2 possess cubic structure with a symmetrical stretching mode of the Ce–O vibrational unit. Fig. 2a shows the Raman peak of sintered CeO_2 pellet, appeared at 463 cm^{-1} and is very sharp and symmetric. Fig. 2b shows the Raman spectra of CeO_2 thin films deposited in the oxygen partial pressure range 2.0×10^{-5}–3.0×10^{-1} mbar. All the films showed peak position ~463 cm^{-1} and is associated with the F_{2g} Raman active mode of polycrystalline cubic structure of CeO_2. The peak ~300 cm^{-1} is due to Si (100) substrate. At base pressure (2.0×10^{-5} mbar), the Raman active mode appeared ~462 cm^{-1} with higher peak intensity and lower FWHM of 13 cm^{-1}. The frequency shift was observed in the range 462–466 cm^{-1}, as the oxygen partial pressure increased from 2×10^{-4} to 3.0×10^{-2} mbar. The FWHM decreased with increasing oxygen partial pressure [23–25]. No peak was observed in the Raman spectrum at 3.0×10^{-1} mbar, due to poor crystallinity and these results are in accordance with XRD results (Fig. 1). The spectra are also prone to be directly affected by the presence of oxygen vacancies. The peak shape becomes broader and asymmetric progressively with increasing oxygen partial pressure. Raman peak broadening indicates the formation of nanocrystalline phase of CeO_2. The Raman study shows the systematic variation in the peak intensity, FWHM and asymmetry with the increase of oxygen partial pressure and is consistent with XRD results. The similar results were also observed by Jonathan et al. [25], Kanakaraju et al. [21] and Wang et al. [23].

3.1.3. High resolution transmission electron microscopy (HRTEM) analysis

The microstructure of CeO_2 film deposited on NaCl single crystal at 3×10^{-2} mbar of oxygen partial pressure and 673 K was analyzed by high resolution transmission electron microscope (HRTEM). Fig. 3a shows the low magnification bright field image of CeO_2 and uniform crystallites distribution. Fig. 3b shows the selected area of electron diffraction (SAED) pattern obtained from CeO_2 film. It showed ring pattern characteristics revealing polycrystalline cubic crystal structure. From the SAED pattern, the lattice vector (G) and then *d* spacings were calculated. The SAED pattern was indexed and it matches with polycrystalline and cubic structure of CeO_2 as shown in Fig. 1. Fig. 3c shows the lattice image of nanocrystalline cubic CeO_2 of (200) orientation. This result confirmed the polycrystalline character of CeO_2 films with (200) preferred orientation and in good agreement with XRD results [26].

3.1.4. Surface morphology analysis

Atomic force microscopy was used to investigate the surface morphology and surface roughness of the films deposited on Si (100). Fig. 4A shows the surface morphology of the films

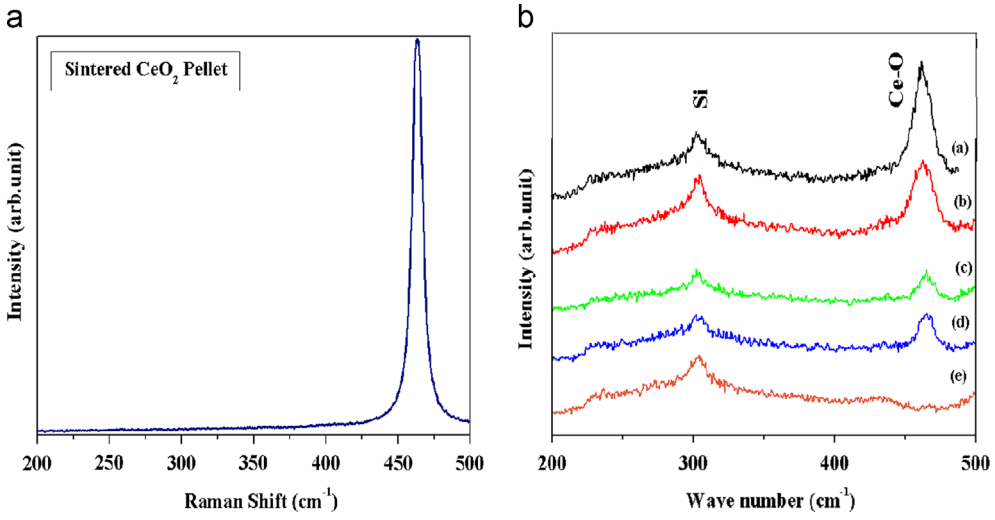

Fig. 2. (a) Raman spectrum of sintered ceria pellet; (b) Raman spectra of ceria thin films prepared at (a) 2.0×10^{-5} mbar; (b) 2×10^{-4} mbar; (c) 3.0×10^{-3} mbar; (d) 3.0×10^{-2} mbar; (e) 3.0×10^{-1} mbar.

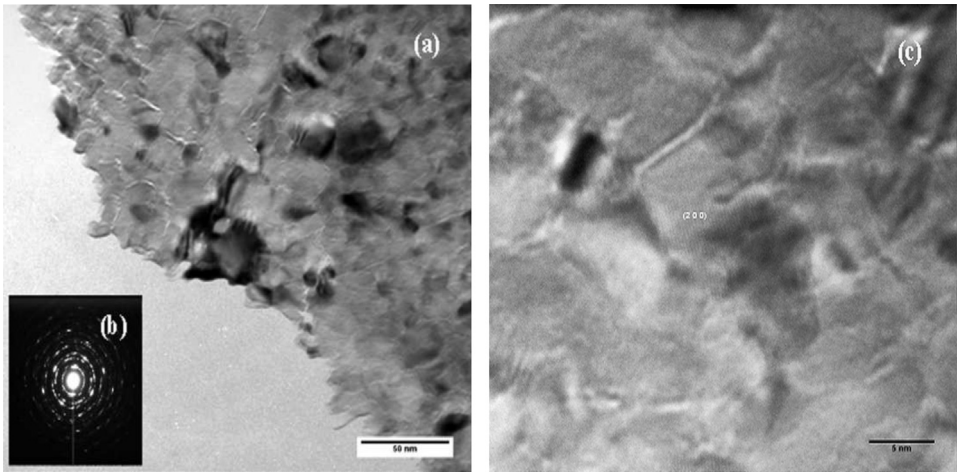

Fig. 3. (a) Low magnification bright field image of ceria film deposited on NaCl substrate at 73 K. (b) Selected Area of Electron Diffraction (SAED) pattern of ceria film. (c) Lattice image from ceria film showing (200) orientation.

prepared at an oxygen partial pressure range 2×10^{-5}–3×10^{-1} mbar. The surface morphology of the films change with thickness, substrate temperature and processing parameters, due to the change of the growth mode [27]. The films showed columnar growth, when the films prepared in the oxygen pressure range 2×10^{-5}–3×10^{-3} mbar. At 3×10^{-2} mbar, the film showed the mixture of columnar and island growth. On increasing the oxygen pressure the columnar growth was observed to be suppressed. Therefore, the oxygen pressure has much influence on the energy of ablated species reaching the substrate and subsequently, the mobility of adatoms on the substrate surface. The other reported results showed that the average energy of ablated particles is almost constant in the pressure range 10^{-5}–10^{-2} mbar, and it decreases considerably in the oxygen pressure $> 10^{-2}$ mbar, due to scattering and collision. Thus, increasing the oxygen pressure more than certain level, lead to deterioration in the crystallinity of films. The surface roughness of the films could be related to many parameters such as substrate temperature, ambient gas, deposition rate, repetition rate, energy density etc. The surface roughness was quantitatively measured by the root-mean-square (RMS) roughness. The surface roughness of the films increased (Fig. 4B) from 0.8 nm to 4.6 nm with increasing oxygen partial pressure from 2×10^{-5} mbar to 3×10^{-1} mbar, owing to the increased crystallinity [28].

3.2. Optical characterization

3.2.1. Photoluminescence spectroscopy

Photoluminescence (PL) spectroscopy was employed to study the optical properties of CeO_2 films deposited on Si (100). CeO_2 films were excited by He–Cd of 325 nm wavelength. The photoluminescence of all the films were measured at room temperature. The PL of CeO_2 films deposited at different oxygen partial pressure is shown in Fig. 5. The PL spectra showed a broad and strong peak ~400 nm and a weak shoulder peak ~442 nm. The PL measurements indicated the oxygen vacancy mediated emission from CeO_2 [29]. The broad PL of the as-deposited films could be the result of defects including oxygen vacancies in the crystal with electronic energy levels below the 4f band. These defects possibly act as recombination centers for electrons initially excited from the valence band to the 4f band of the oxide [29,30]. The peak intensity of PL spectra of these samples decreased with increasing oxygen partial pressure, due to reduction in the concentration of O_2 related defects.

We noticed a broad PL peak at an energy value of 3.05 eV (~ 408 nm) for the films deposited in the oxygen pressure range 2×10^{-5}–3×10^{-3} mbar. It is found that the bandgap values increased from 3.05 eV to 3.1 eV as the oxygen pressure increased from 2×10^{-5} to 3×10^{-1} mbar. There are defect energy levels between Ce4f and O2p level, so wide PL peaks could be observed. It was inferred that the PL of CeO_2 is due to the transition by Ce4f → O2p and defects level → O2p [31,32]. These defects levels are located in the range of 1 eV around Ce4f band. The peak ~400 nm could be due to either 5d to 4f or 4f to valence band transitions [33] and coincides in energy with the 4f to valence band energy gap of 3.1 eV obtained from optical absorption measurements on CeO_2 reported in the literature [34–36]. Giardini Guidoni et al. [36] deposited CeO_2 films on glass substrates at 400 °C by PLD and found that the energy bandgap of 3.1 eV. Ghanashyam Krishna et al. [37] revealed that the pure CeO_2 exhibited the bandgap of 3.3 eV at 873 K. Ozer [5] prepared the CeO_2 films and found the optical bandgap value of 3.1 eV. Choudhury and Choudhury [38] prepared pure and doped CeO_2 nanoparticles and found the band to band excitation peak at 408 nm. Ansari [30] prepared the CeO_2 films and found the strong band ~378 nm in the photoluminescence spectra, correspond to the direct bandgap of 3.23 eV. These reported results are consistent with present results.

3.2.2. UV–visible spectroscopy studies

The refractive indices were calculated from the transmission spectra of CeO_2 films deposited on glass substrates at different oxygen partial pressure [28]. The refractive indices of the films decreased from 2.41 to 1.72 (at 550 nm wavelength) with increasing oxygen partial pressures and the values are given in Table 1. The variation of refractive indices is due to the

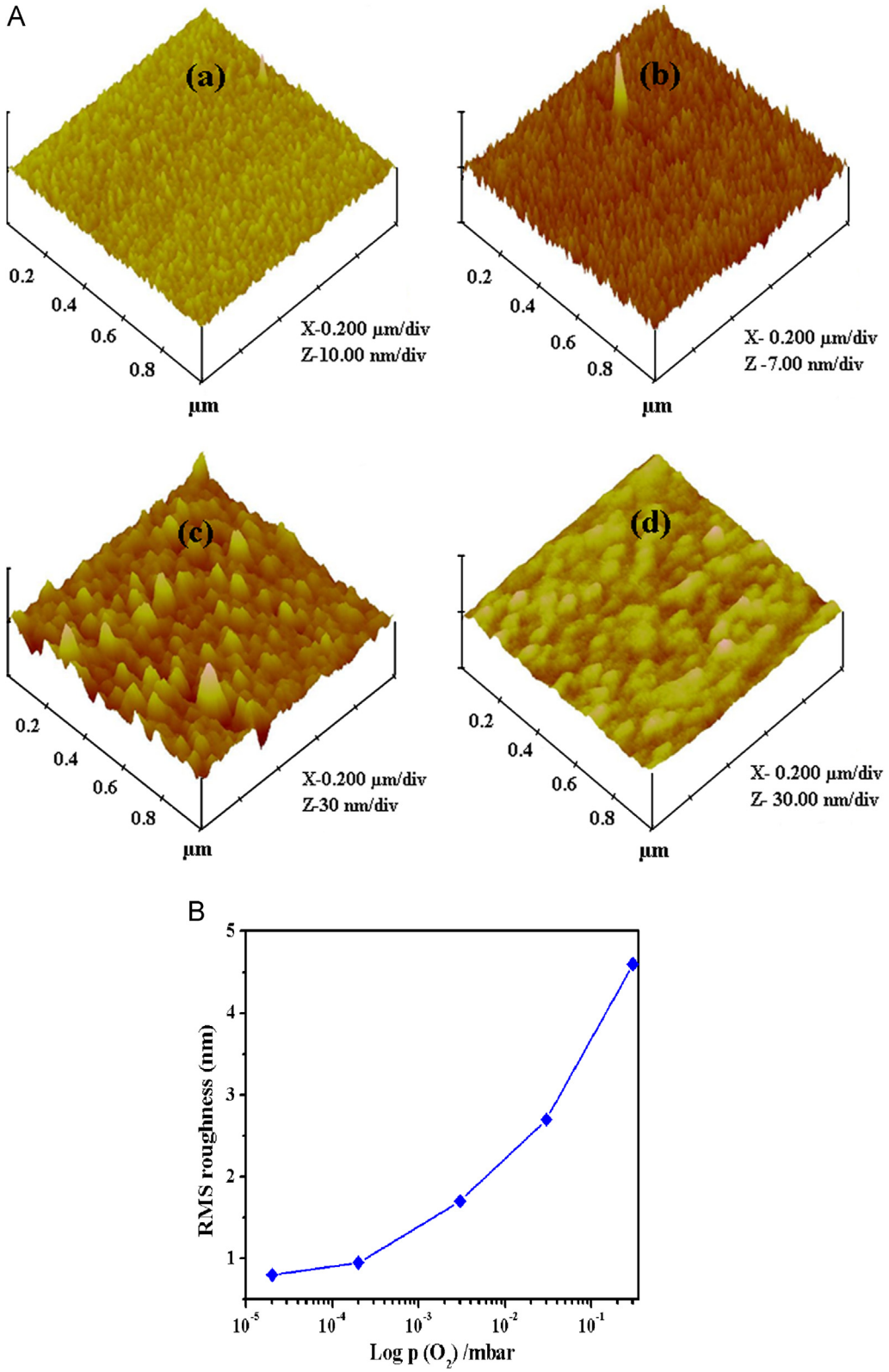

Fig. 4. (A) AFM images ($1 \times 1\ \mu m^2$) of the CeO_2 films deposited at different oxygen partial pressures: (a) 2×10^{-5} mbar; (b) 3×10^{-3} mbar; (c) 3×10^{-2} mbar; (d) 3×10^{-1} mbar. (B) RMS roughness of the films deposited as a function of oxygen partial pressure.

variation of packing density of the films. The packing density of the films depends on the energy of the ablated species. It is possible to correlate the oxygen partial pressure with the difference in the energy of the ablated species. At higher oxygen partial pressure, the energy of the ablated species is lower due to scattering and multiple collisions, causes films of lower thickness and packing density with rougher surfaces resulting lower refractive indices. Therefore, the higher oxygen

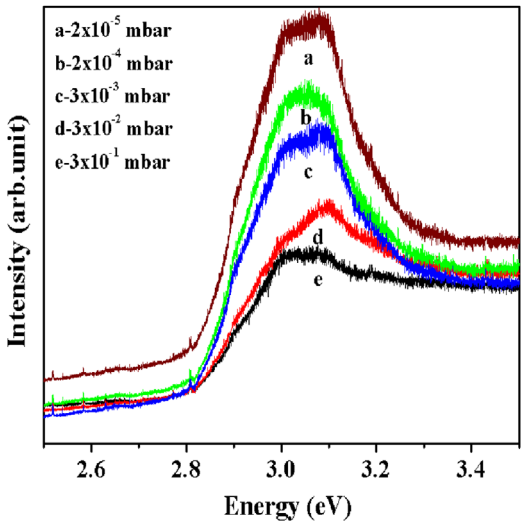

Fig. 5. PL spectra of CeO_2 films deposited at various oxygen partial pressures and 673 K.

partial pressure causes lower packing density, whereas at lower oxygen partial pressure the energy of the species is higher, which leads to higher packing density of the films. Hence the refractive indices decreased with increasing oxygen partial pressure. The results from UV–visible spectrophotometer analysis showed that the optical properties of the films was influenced by the oxygen partial pressure [28,39,40]. The present investigation showed that the structure, preferred orientation, surface morphology and optical properties of the CeO_2 films could be controlled by a proper selection of the oxygen partial pressure, resulting high packing density and hence it can be used for optical applications.

4. Conclusions

The CeO_2 films were deposited on Si (100) and glass substrates with various oxygen partial pressures at a substrate temperature of 673 K by PLD. The XRD results showed that the films were polycrystalline cubic structure with (200) preferred orientation. The Raman peak $\sim$463 cm^{-1} indicated the F_{2g} active mode of CeO_2 with a cubic structure. The HRTEM analysis confirmed the polycrystalline and cubic nature of CeO_2 films with (200) orientation. The AFM investigation indicated the change of growth mode of the films from columnar to island with increasing oxygen partial pressure range 2×10^{-5}–3×10^{-1} mbar. The optical studies indicated that the optical bandgap values increased from 3.05 to 3.1 eV and the refractive indices decreased from 2.41 to 1.72 (at 550 nm wavelength) with increasing oxygen partial pressures.

Acknowledgment

The authors (G.B, J.I.S and S.I.B) are thankful to the National Research Foundation of Korea (NRF) for the grant funded by the Korea Government (MEST) (No.2012-0009455) for this research work.

References

[1] P. Patsalas, S. Logothetidis, C. Metaxa, Optical performance of nanocrystalline transparent ceria films, Applied Physics Letters 81 (2002) 466–468.
[2] F.C. Chiu, C.M. Lai, Optical and electrical characterizations of cerium oxide thin films, Journal of Physics D: Applied Physics 43 (2010) 075104-1–075104-5.
[3] S.N. Jacobsen, L.D. Madsen, U. Helmersson, Epitaxial cerium oxide buffer layers and $YBa_2Cu_3O_{7-\delta}$ thin films for microwave device applications, Journal of Materials Research 14 (1999) 2385–2393.
[4] T. Inoue, M. Osonoe, H. Tohda, M. Hiramatsu, Y. Yamamoto, A. Yamanaka, T. Nakayama, Low temperature epitaxial growth of cerium dioxide layers on silicon, Journal of Applied Physics 69 (1991) 8313–8315.
[5] Nilgün Özer, Optical properties and electrochromic characterization of sol–gel deposited ceria films, Solar Energy Materials and Solar Cells 68 (2001) 391–400.
[6] Piotr Jasinski, Toshio Suzuki, Harlan U. Anderson, Nanocrystalline undoped ceria oxygen sensor, Sensors and Actuators B: Chemical 95 (2003) 73–77.
[7] R. Thanneeru, S. Patil, S. Deshpande, S. Seal, Effect of trivalent rare earth dopants in nanocrystalline ceria coatings for high-temperature oxidation resistance, Acta Materialia 55 (2007) 3457–3466.
[8] Kai Wang, Alla Reznik, Karim S. Karim, SPIE Proceedings: Optical Materials and Structures Technologies IV, in: Joseph L. Robichaud, William A. Goodman, (Eds.) vol. 7425.
[9] Dimple P. Dutta, N. Manoj, A.K. Tyagi, White light emission from sonochemically synthesized rare earth doped ceria nanophosphors, Journal of Luminescence 131 (2011) 1807–1812.
[10] E.C.C. Souza, H.F. Brito, E.N.S. Muccillo, Optical and electrical characterization of samaria-doped ceria, Journal of Alloys and Compounds 491 (2010) 460–464.
[11] K. Konstantinov, I. Stambolova, P. Peshev, B. Darriet, S. Vassilev, Preparation of ceria films by spray pyrolysis method, International Journal of Inorganic Materials 2 (2000) 277–280.
[12] M.S. Anwar, Shalendra Kumar, Faheem Ahmed, Nishat Arshi, Yong Jun Seo, Lee Chan Gyu, Bon Heun Koo, Study of nanocrystalline ceria thin films deposited by e-beam technique, Current Applied Physics 11 (2011) S301–S304.
[13] M.T. Ta, D. Briand, Y. Guhel, J. Bernard, J.C. Pesant, B. Boudart, Growth and structural characterization of cerium oxide thin films realized on Si (111) substrates by on-axis r.f. magnetron sputtering, Thin Solid Films 517 (2008) 450–452.
[14] I. Zhitomirsky, A. Petric, Electrochemical deposition of ceria and doped ceria films, Ceramics International 27 (2001) 149–155.
[15] G. Balakrishnan, S. Tripura Sundari, P. Kuppusami, P. Chandra Mohan, M.P. Srinivasan, E. Mohandas, V. Ganesan, D. Sastikumar, A study of microstructural and optical properties of nanocrystalline ceria thin films prepared by pulsed laser deposition, Thin Solid Films 519 (2011) 2520–2526.
[16] G. Balakrishnan, P. Kuppusami, T.N. Sairam, R. Thirumurugesan, E. Mohandas, D. Sastikumar, Synthesis and properties of ceria thin films prepared by pulsed laser deposition, Journal of Nanoscience and Nanotechnology 9 (2009) 5421–5424.
[17] D.B. Chrisey, G.B. Hubler, in: Pulsed Laser Deposition of Thin Films, Wiley, New York, 1994.
[18] B. Elidrissi, M. Addou, M. Regragui, C. Monty, A. Bougrine, A. Kachouane, Structural and optical properties of CeO_2 thin films prepared by spray pyrolysis, Thin Solid Films 379 (2000) 23–27.
[19] I. Porqueras, C. Pearson, C. Corbella, M. Vives, A. Pinyol, E. Bertran, Characteristics of e-beam deposited electrochromic CeO_2 thin films, Solid State Ionics 165 (2003) 131–137.
[20] R.P. Wang, S. Pan, Y. Zhou, G. Zhou, N. Liu, K. Xie, H. Lu, Fabrication and characteristics of CeO_2 films on Si (100) substrates by pulsed laser deposition, Journal of Crystal Growth 200 (1999) 505–509.
[21] S. Kanakaraju, S. Mohan, A.K. Sood, Optical and structural properties of reactive ion beam sputter deposited CeO_2 films, Thin Solid Films 305 (1997) 191–195.

[22] S. Amirhaghi, I.W. Boyd, Y.H. Li, J.A. Kilner, Growth of pure and doped cerium oxide thin-film bilayers by pulsed-laser deposition, Materials Science and Engineering B 34 (1995) 192–198.
[23] Shengyue Wang, Wei Wang, Jian Zuo, Yitai Qian, Study of the Raman spectrum of CeO_2 nanometer thin films, Materials Chemistry and Physics 68 (2001) 246–248.
[24] Igor Kosacki, Toshio Suzuki, Harlan U. Anderson, Philippe Colomban, Raman scattering and lattice defects in nanocrystalline CeO_2 thin films, Solid State Ionics 149 (2002) 99–105.
[25] Jonatham E. Spanier, Richard D. Robinson, Feg Zhang, Siu-Wai Chan, Irving P. Herman, Size-dependent properties of CeO_{2-y} nanoparticles as studied by Raman scattering, Physical Review B 64 (2001) 245407-1–245407-8.
[26] S. Logothetidis, P. Patsalas, E.K. Evangelou, N. Konofaos, I. Tsiaoussis, N. Frangis, Dielectric properties and electronic transitions of porous and nanostructured cerium oxide films, Materials Science and Engineering B 109 (2004) 69–73.
[27] D.Q. Shi, M. Ionescu, T.M. Silver, S.X. Dou, Relationship between epitaxial deposition and growth modes of CeO_2 films, Physica C 384 (2003) 475–481.
[28] G. Balakrishnan, T.N. Sairam, P. Kuppusami, R. Thiumurugesan, E. Mohandas, V. Ganesan, D. Sastikumar, Influence of oxygen partial pressure on the properties of pulsed laser deposited nanocrystalline zirconia thin films, Applied Surface Science 257 (2011) 8506–8510.
[29] M.Y. Chen, X.T. Zu, X. Xiang, H.L. Zhang, Effects of ion irradiation and annealing on optical and structural properties of CeO_2 films on sapphire, Physica B: Condensed Matter 389 (2007) 263–268.
[30] Anees A. Ansari, Optical and structural properties of sol–gel derived nanostructured CeO_2 film, Journal of Semiconductors 31 (2010) 053001-1–053001-5.
[31] V.V. Ursaki, V. Lair, L.Z. Ivkovic, M. Cassir, A. Ringuede, O. Lupan, Optical properties of Sm-doped ceria nanostructured films grown by electrodeposition at low temperature, Optical Materials 34 (2012) 1897–1901.
[32] Chai Chunlin, Yang Shaoyan, Liu Zhikai, Liao Meiyong, Chen Nuofu, Violet/blue photoluminescence from CeO_2 thin film, Chinese Science Bulletin 48 (2003) 1198–1200.
[33] C.A. Hogarth, Z.T. Al-Dhhan, Optical absorption in thin films of cerium dioxide and cerium dioxide containing silicon monoxide, Physica Status Solidi B 137 (1986) K157–K160.
[34] C.W. Sun, H. Li, H.R. Zhang, Z.X. Wang, L.Q. Chen, Controlled synthesis of CeO_2 nanorods by solvothermal method, Nanotechnology 16 (2005) 1454–1463.
[35] Sumalin Phoka, Paveena Laokul, Ekaphan Swatsitang, Vinich Promarak, Supapan Seraphin, Santi Maensiri, Synthesis, structural and optical properties of CeO_2 nanoparticles synthesized by a simple polyvinyl pyrrolidone (PVP) solution route, Materials Chemistry and Physics 115 (2009) 423–428.
[36] A. Giardini Guidoni, C. Flamini, F. Varsano, M. Ricci, R. Teghil, V. Marotta, T.M. Di Palma, Ablation of transition metal oxides by different laser pulse duration and thin films deposition, Applied Surface Science 154–155 (2000) 467–472.
[37] M. Ghanashyam Krishna, A. Hartridge, A.K. Bhattacharya, Temperature and ionic size dependence of the properties of ceria based optionic thin films, Materials Science and Engineering B 55 (1998) 14–20.
[38] Biswajit Choudhury, Amarjyoti Choudhury, Lattice distortion and corresponding changes in optical properties of CeO_2 nanoparticles on Nd doping, Current Applied Physics 13 (2013) 217–223.
[39] Enrique Ruiz-Trejo, The optical band gap of Gd-doped CeO_2 thin films as function of temperature and composition, Journal of Physics and Chemistry of Solids 74 (2013) 605–610.
[40] G. Balakrishnan, P. Kuppusami, S. Tripura Sundari, R. Thirumurugesan, V. Ganesan, E. Mohandas, D. Sastikumar, Structural and optical properties of γ-alumina thin films prepared by pulsed laser deposition, Thin Solid Films 518 (2010) 3898–3902.